

Weighted persistent homology for osmolyte molecular aggregation and hydrogen-bonding network analysis

D Vijay Anand¹, Kelin Xia^{1,2*}, Yuguang Mu^{1,2}

¹Division of Mathematical Sciences, School of Physical and Mathematical Sciences, Nanyang Technological University, Singapore 637371

²School of Biological Sciences, Nanyang Technological University, Singapore 637371

July 16, 2019

Abstract

It has long been observed that trimethylamin N-oxide (TMAO) and urea demonstrate dramatically different properties in a protein folding process. Even with the enormous theoretical and experimental research work of the two osmolytes, various aspects of their underlying mechanisms still remain largely elusive. In this paper, we propose to use the weighted persistent homology to systematically study the osmolytes molecular aggregation and their hydrogen-bonding network from a local topological perspective. We consider two weighted models, i.e., localized persistent homology (LPH) and interactive persistent homology (IPH). Similar to our previous works, we use persistent Betti number (PBN) and persistent entropy (PE) to quantitatively characterize the topological features from LPH and IPH. More specifically, from the localized persistent homology models, we have found that TMAO and urea have very different local topology. TMAO shows local network structures. With the concentration increase, the circle elements in these networks show a clear increase in their total numbers and a decrease in their relative sizes. In contrast, urea shows two types of local topological patterns, i.e., local clusters around 6 Å and a few global circle elements at around 12 Å. From the interactive persistent homology models, it has been found that our persistent radial distribution function (PRDF) from the global-scale IPH has same physical properties as the traditional radial distribution function (RDF). Moreover, PRDFs from the local-scale IPH can also be generated and used to characterize the local interaction information. Other than the clear difference of the first peak value of PRDFs at filtration size 4Å, TMAO and urea also shows very different behaviors at the second peak region from filtration size 5Å to 10 Å. These differences are also reflected in the PBNs and PEs of the local-scale IPH. These localized topological information has never been revealed before. Other than the osmolyte systems, our weighted persistent homology models can also be used to analyze any types of networks, graphs, molecular structures, etc.

Key words: Persistent homology, Molecular aggregation, Hydrogen-bonding network, Persistent Betti number, Persistent entropy.

*Address correspondences to Kelin Xia. E-mail:xiakelin@ntu.edu.sg

1 Introduction

Tri-methylamine N-oxide (TMAO) and urea are organic osmolytes widely existing in the animal metabolisms. Deep-sea organisms use the protein stabilizing effects of TMAO to counteract the high pressure perturbation, while mammalian kidneys use the strong denaturant function of urea.⁹³ As a protecting osmolyte, TMAO can counteract the urea protein-denaturing effects. Currently, it is well accepted that urea acts by directly binding to the protein backbones and side chains.⁴⁹ It has very little disturbance to the surrounding water structures. TMAO’s stabilization is not well understood. It has been suggested that TMAO form complexes with two to three water molecules, and protein stabilization is the result of depletion effects associated with unfavorable interaction of TMAO with protein backbone.⁵⁹ Others suggest that TMAO interacts with polypeptides and protein stabilization is a result of surfactant-like effects of TMAO.⁶⁴ The interaction between TMAO and urea is also not well understood.⁵¹ Even though it is suggested that the interaction is through the TMAO’s modification of urea-water structures, recent experiments show that the addition of TMAO induces blue shifts in urea’s H-N-H symmetric bending modes, indicating the direct interactions between the two cosolvents.^{114, 116} Although great progress has been made in both experimental and theoretical research for urea and TMAO,^{6-8, 50, 60, 67, 79, 80, 87, 89, 90, 98, 99} the detailed mechanism for their molecular aggregations and corresponding hydrogen-bonding networks still remain elusive.

Theoretically, graph or network based models,^{39, 77, 85} especially the spectral graph models and combinatorial graph models, play the key role in the characterization of biomolecular structures, interaction networks, hydrogen-bonding network, etc.^{4, 5, 32-36} The most commonly-used graph-based measurements include, node degree, shortest path, clique, cluster coefficient, closeness, centrality, betweenness, Cheeger constant, modularity, graph Laplacian, graph spectral, Erdős number, percolation information, etc. Differential geometry tools,^{9, 28, 29, 41, 46, 82, 96, 106} such as Voronoi diagram, alpha shape, geometric flows, etc, have also been considered to quantitatively characterize biomolecular structure, surface, volume, cavity, void, tunnels, interface, etc. Recently, a new topological model known as persistent homology has demonstrated a great promise in biomolecular structure, flexibility, dynamics and function analysis.^{101, 107, 109, 111, 112} Persistent homology based machine learning and deep learning models⁸⁴ have achieved great successes in protein-ligand binding affinity prediction,^{23, 24, 75} protein stability change upon mutation^{21, 22} and toxicity prediction.¹⁰³ These topology based machine learning models have constantly achieved some of the best results in D3R Grand challenge.⁷⁴ Motivated by the great success of topological modeling in biomolecules, we have applied persistent homology in the analysis of ion aggregations and hydrogen-bonding networks.¹⁰⁴ The two types of ion aggregation models, i.e., local clusters and extended ion networks, can be well characterized by our model. Further, we have identified, for the first time, two types topology for the two hydrogen-bonding network systems.¹⁰⁴ More recently, we study the osmolyte molecular aggregation and their hydrogen-bonding networks. Two osmolytes, i.e., TMAO and urea, are found to share very similar topological patterns with the two types of ion systems, i.e., KSCN and NaCl. Particularly, the topological fingerprints for the hydrogen-bonding network from ion systems and osmolyte systems share a great similarity. This indicates that our topological representation can characterize certain intrinsic difference between “structure making” and “structure breaking” systems.

More recently, weighted persistent homology (WPH) models have been proposed to incorporate physical, chemical and biological properties into topological modeling.⁶⁸ Essentially, the weight value, which reflects physical, chemical and biological properties, can be assigned to vertices (atom centers), edges (bonds), or higher order simplexes (cluster of atoms), depending on the biomolecular structure, function, and dynamics properties.⁶⁸ In this way, weighted persistent homology can be characterized into three major categories, i.e., vertex-weighted,^{11, 20, 40, 54, 111, 113} edge-weighted,^{17, 21, 24, 83, 110, 111} and simplex-weighted models.^{37, 86, 102} Among them, the localized (weighted) persistent homology (LPH) and interactive persistent homology (IPH) are found to be of great importance in the classification and clustering of DNA structures and trajectories,⁶⁸ and protein ligand interactions.²¹

In this paper, for the first time, we apply the localized persistent homology and interactive persistent homology in the study of osmolyte molecular aggregation and their hydrogen-bonding networks. Similar to our previous works, we use persistent Betti number (PBN) and persistent entropy (PE) to quantitatively characterize the topological features from LPH and IPH. More specifically, using LPH, we have revealed that TMAO and urea have very different local topologies. Local network structures are observed in TMAO systems. With the concentration increase, the circles within these networks show a huge increase in their

total numbers and a sharp decrease in their relative sizes. In contrast, urea shows two distinguishable local topological features, i.e., local clusters around 6 Å and global-scale circle structures at around 12 Å. Further, we have demonstrated that our global-scale IPH based persistent radial distribution function (PRDF) is similar to the traditional radial distribution function (RDF) and can be used to characterize the double layer information. Moreover, a new local-scale PRDFs can be generated from our local-scale IPH model. Essentially, in global-scale IPH, each osmolyte molecule interacts with all the water molecules in the systems. However, in global-scale IPH, water molecules are classified into different cells based on the Voronoi diagram of osmolyte molecules. The interaction happens between the osmolyte molecule and the water molecules within its Voronoi cell and between two closest Voronoi cells. This classification is naturally embedded in the filtration process of IPH analysis. Further, IPH based PBNs and PEs can also be used to study the interaction patterns between osmolyte molecules and water molecules. Other than the osmolyte systems, our weighted persistent homology models can also be used to analyze networks, graphs, biomolecules, etc.

The paper is organized as follows. A brief introduction of persistent homology and two weighted persistent homology models are given in Section 2. The main results are presented in Section 3. The LPH based molecular aggregation and hydrogen-bonding networks is discussed in Section 3.2. The IPH based topological features for osmolyte-water interaction networks are discussed in Section 3.3. The paper ends with a conclusion.

2 Theory and models

In this section, we will give a brief introduction of persistent homology and weighted persistent homology. Three types of persistent functions, including persistent Betti number, persistent entropy and persistent radial base function, will be discussed in details. A general description of the two WPH models, i.e., localized persistent homology and interactive persistent homology, will also be presented.

2.1 Persistent homology

Persistent homology has been proposed to study the “shape” of data. It has become more and more popular in a variety of fields, including shape recognition,³⁸ network structure,^{57,63,94} image analysis,^{13,26,47,78,95} data analysis,^{25,65,76,88,100} chaotic dynamics verification,⁷⁰ computer vision,⁹⁵ computational biology,^{48,61,115} amorphous material structures,^{56,92} etc. Researchers have developed many elegant softwares, including JavaPlex,⁹⁷ Perseus,⁷³ Dipha,¹⁰ Dionysus,¹ jHoles,¹⁷ GUDHI,⁶⁶ etc.⁴⁴ Visualization methods, including persistent diagram,⁷¹ persistent barcode,⁵² and persistent landscape,^{18,19} have also been proposed. In this section, we only present a brief introduction of persistent homology. A more detailed description of its mathematical background can be found in references.^{27,42,117}

Persistent homology studies the topological invariant called Betti numbers, which include β_0 , β_1 , β_2 , etc. Geometrically, β_0 represents the number of connected components, β_1 represents the number circles, rings or loops, and β_2 represents the number of voids or cavities. Persistent homology enables a multiscale representation of topological invariants from simplicial complexes. Generally speaking, a network or graph is a special kind of simplicial complex with only 0-simplexes (nodes or vertexs) and 1-simplexes (edges). Simplicial complexes can have higher-dimensional components,⁵³ such as 2-simplexes and 3-simplexes, which can be geometrically viewed as triangles and tetrahedrons, respectively. Moreover, the key concept in persistent homology is the filtration. For example, if we have a point cloud data, we can associate each point with an identical-sized sphere and assign its radius as the filtration parameter. With the increase of filtration value, these spheres will systematically enlarge and further overlap with each other to form simplexes. Roughly speaking, an edge between two points is formed when the two corresponding spheres overlap. A triangle is formed when each of two spheres (of the three corresponding spheres from triangle vertices) overlap. And a tetrahedron is formed when each three spheres (of the four corresponding spheres from tetrahedron vertices) overlap. At each filtration value, all the simplexes, i.e., vertices, edges, triangles, tetrahedrons, form a simplicial complex. From it, topological invariants, i.e., Betti numbers, can be calculated. Through a systematical variation of a filtration parameter, a series of simplicial complexes from different scales are generated. Some topological invariants persistent longer in these simplicial complexes, while others quickly disappear when the filtration value changes. In this way, the “lifespan” of the topological invariants (circles, loops, etc) in these simplicial complexes provides a natural geometric measurement. More specifically, the lifespan, known as the persistence, measures how “large” are the circles, loops and voids in the system.

We call a filtration value, at which a topological invariant appears or disappears, birth time (BT) and

death time (DT), respectively. In this way, each topological invariant has a “lifespan” defined by its birth and death time. Essentially, the lifespan provides a geometric measurement of the topological invariant. If we use a one-dimensional bar, started at BT and ended at DT, to represent each homology generator, a barcode representation is generated. We can denote barcodes as follows,

$$\{L_{k,j} = [a_{k,j}, b_{k,j}] | k = 0, 1, \dots; j = 1, 2, 3, \dots, N_k\}, \quad (1)$$

where parameter k represents the k -th dimension. For data points located in Euclidean space, normally we only consider $k = 0, 1, 2$. Parameter j indicates the j -th topological invariant and N_k is the number of β_k topological invariant. The $a_{k,j}$ and $b_{k,j}$ are BTs and DTs. For simplification, we can define the set of k -th dimensional barcodes as,

$$L_k = \{L_{k,j}, j = 1, 2, 3, \dots, N_k\}, \quad k = 0, 1, \dots$$

Various functions can be defined on the barcodes.

Persistent Betti number Based on the persistent homology results, different functions are proposed to represent or analyze the topological information.^{18,25,31,42} Among them is the persistent Betti number (PBN), which is defined as the summation of all the k -th dimensional barcodes,

$$f(x; L_k) = \sum_j \chi_{[a_{k,j}, b_{k,j}]}(x), \quad k = 0, 1, \dots \quad (2)$$

Function $\chi_{[a_{k,j}, b_{k,j}]}(x)$ is a step function, which equals to one in the region $[a_{k,j}, b_{k,j}]$ and zero elsewhere. This equation transforms the k -dimensional barcodes into a one-dimensional function. We can also define an average PBN as follows,

$$f(x; L_k) = \frac{1}{N} \sum_j \chi_{[a_{k,j}, b_{k,j}]}(x), \quad k = 0, 1, \dots \quad (3)$$

Note that N can be the total number of atoms, β_k bars (N_k), or other measurements.

Persistent entropy Persistent entropy (PE) has been proposed^{31,69,91,108} to measure the system disorder. For the k -th dimensional barcodes, it is defined as,

$$S_k = \sum_j^{N_k} -p_{k,j} \ln(p_{k,j}), \quad k = 0, 1, \dots, \quad (4)$$

with the probability function,

$$p_{k,j} = \frac{b_{k,j} - a_{k,j}}{\sum_j (b_{k,j} - a_{k,j})}, \quad k = 0, 1, \dots \quad (5)$$

The expression of PE can be simplified as follows,

$$S_k = \ln \left(\sum_j^{N_k} (b_{k,j} - a_{k,j}) \right) - \frac{\sum_j^{N_k} ((b_{k,j} - a_{k,j}) \ln(b_{k,j} - a_{k,j}))}{\sum_j^{N_k} (b_{k,j} - a_{k,j})}, \quad k = 0, 1, \dots \quad (6)$$

It should be noticed that PE is different from the general entropy used in molecular dynamic simulation. Generally speaking, PE characterizes the “topological regularity”. For instance, crystals have very consistent three-dimensional structures. They will generate highly regular barcodes thus a large PE value. Topologically, a large PE value means that the structure is more regular and “lattice-like”, while a lower PE value means the components in the structure are randomly distributed with no consistent patterns.

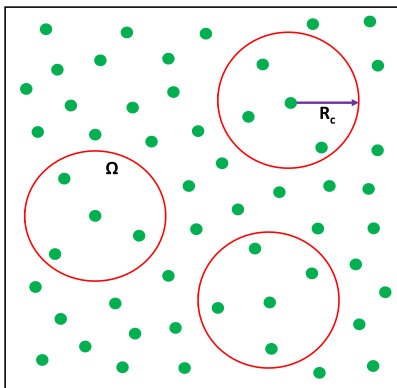


Figure 1: A schematic representation of the localized persistent homology (LPH) analysis. The red circle (a sphere in 3D) specifies the local region. Persistent homology is carried out on all the molecules within the local region.

Persistent radial distribution function Based on the β_0 barcode, we propose the persistent radial distribution function (PRDF) as follows,

$$f(x; L_0) = \frac{x_t}{N_0} \sum_j \frac{\delta(x - b_{0,j})}{4\pi x^2}. \quad (7)$$

Here x_t is the filtration value when the PBN reduces to one, i.e., only one connected component. Integer N_0 is the total number of β_0 bars. Essentially, if we consider the global interactive persistent homology, our PRDF will result in the common RDF.³⁰ If we use the local interactive persistent homology, our PRDF will focus on the interaction within each cell of the Voronoi diagram. Detailed discussion is given in Section 2.2.2.

2.2 Weighted persistent homology

Weighted persistent homology models have been proposed to incorporate physical, chemical and biological properties into topological modeling.⁶⁸ They can also be designed to characterize local topological information and certain special interaction patterns. In this paper, we will focus on two WPH models, i.e., localized persistent homology and interactive persistent homology.

2.2.1 Localized persistent homology

The design of our LPH model is greatly inspired by the great success of element specific persistent homology (ESPH).^{23,24} Different from all previous topological models, which consider the data/structure as an inseparable system, ESPH decomposes the data/structure into a series of subsets made of certain type(s) of atoms, which have been found to characterize very well various biological properties, such as hydrophobic or hydrophilic interactions.^{21–24,74,75,103} Moreover, our LPH model is very different from traditional persistent local homology (PLH).^{3,12,14,15,45,72} Mathematically, PLH model studies the relative homology groups between a topological space and its subspace, while LPH explores the homology groups from local topology. Previously, LPH was used to characterize local topological features of biomolecular structure or complexes.⁶⁸ In LPH, the structure is decomposed into a series of local domains or regions, that may overlap with each other, and persistent homology analysis is then systematically applied on part (or all) of these local domains or regions. In this paper, our main focus is to characterize the local features, such as ion clustering, double layer, local aggregations, etc, that are widely existed in ion or molecular aggregation and hydrogen-network systems.

Mathematically, the global persistent homology analysis studies the whole system, while the localized persistent homology is performed on a local region, domain or subspace. In the current paper, we define the subspace as a sphere with radius (R_c). More specifically, a sphere of radius R_c is considered around each molecule (either osmolyte or water molecule) and only the molecules within this sphere are chosen for the localized persistent homology analysis. Figure 1 shows a schematic configuration in which a particular

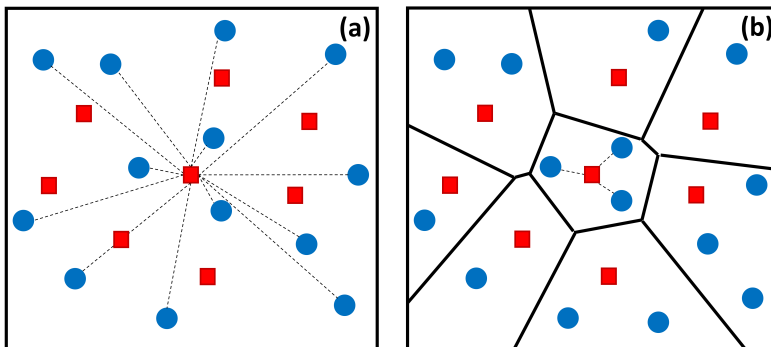


Figure 2: Illustration of interactions in global-scale and local-scale interactive persistent homology (IPH). In global-scale IPH model, an osmolyte molecule (red rectangle) interacts with all the water molecules (blue dots). In local-scale model, an osmolyte molecule (red rectangle) interact only with water molecules (blue dots) in its Voronoi cell, and Voronoi cell-cell interactions happen only between closest neighbours.

molecule is selected and a sphere of radius R_c is drawn around it. The molecules within this enclosure are chosen as the local neighbors of the central molecule. The persistent homology analysis is carried out for the selected molecules to generate the local persistent barcodes. This procedure is repeated for each molecule in the configuration. In other words, each molecule in a given configuration is associated with its local neighbors which dictate its local structure.

2.2.2 Interactive persistent homology

The interactive persistent homology (IPH) is proposed to study the interaction between proteins and ligands.²¹ The essential idea is to study the topological invariant of the interaction networks, which are formed between protein atoms and ligand atoms. More specifically, for a protein-ligand complex, an interaction matrix can be built with its element as the Euclidean distance between two atoms. However, if two atoms come from the same molecule (either protein or ligand), its distance is set to infinity, meaning they will never interact in IPH. In this way, the IPH model can be used in the characterization of the protein-ligand interactions. Actually, IPH based machine learning models are found to deliver the best results in protein-ligand binding affinity prediction.^{21, 22, 74}

In this section, we use IPH models to characterize the interactions between osmolyte and water molecules. Two different models, i.e., global-scale IPH and local-scale IPH, are considered. In global-scale model, when an osmolyte molecule is selected and the distances (d_{ij}) between all water molecules to this osmolyte molecule are considered. More specifically, suppose there are N_{wtr} number of water molecules, a global-scale IPH matrix of size $(N_{wtr} + 1) \times (N_{wtr} + 1)$ can be constructed between a selected osmolyte molecule and all water molecules as follows,

$$M_{ij} = \begin{cases} d_{ij}, & \text{if } T_{type}(i) \neq T_{type}(j); \\ \infty, & \text{otherwise} \end{cases} \quad (8)$$

Here $T_{type}(i)$ is used to tell if the i -th molecule is osmolyte or water, i.e., type of the molecule. If there are N_{sml} number of osmolyte molecule, we can construct a total N_{sml} number of gloabl-scale IPH matrixes. From these matrixes, PRDF as in Eq. (7) can be calculated and the average of these PRDFs will characterize the same physical properties as the traditional radial distribution function.³⁰

In local-scale IPH, a similar IPH matrix as in Eq.(8) is considered. But this new IPH matrix is now of size $(N_{wtr} + N_{sml}) \times (N_{wtr} + N_{sml})$, meaning all distances between water and osmolyte molecules are considered simultaneously. The new IPH matrix based filtration characterizes dramatically different topological information. More specifically, molecules with shorter distances to their neighbors will form connections at earlier

stage of the filtration. In this way, a Voronoi diagram will naturally form when water molecules connect to their center osmolyte molecule. Later, Voronoi cells will merge with closest neighbors to become a well-connected entity. The β_0 barcodes capture very well the above topological information. And the corresponding PRDFs describe the local interactions within the Voronoi cells.

A comparison between global-scale and local-scale IPH is illustrated in Figure 2. Essentially, each osmolyte molecule can interact directly with all water molecules in global-scale model and the resulting PRDF (from β_0 barcodes) characterizes the same physical properties as RDF. In local-scale IPH model, only the interactions between the osmolyte molecule and water molecules in its Voronoi cell, and the Voronoi cell-cell interactions are captured in β_0 bars. It should be noticed that the corresponding PRDFs only describe the local interaction information, and they are very different from the traditional RDF.

3 Results and discussions

We use the weighted persistent homology models to investigate the local topological structure of two osmolytes, namely, trimethylamin N-oxide (TMAO) and urea. Two models, i.e., localized persistent homology and interactive persistent homology, are used to reveal the local topological features in the aggregation, hydrogen networks, and their interactions.

3.1 MD simulation and data generation

We consider the same molecular dynamics (MD) setting as in the paper.¹⁰⁵ More specifically, we consider GROMACS-5.1.2^{2,16} for the MD simulation. The four point (TIP4P-EW)⁵⁸ water model are used, and Kast model⁶² is adopted for TMAO whereas the urea model is from AMBER package.⁸¹ Two osmolytes with eight different concentrations, from 1M to 8M, in pure water are studied, respectively. To construct the initial state, urea/TMAO molecules are randomly distributed using insert-molecules utility in GROMACS, after that 3000 water molecules are inserted randomly into the cubic simulation box. We carry out the equilibration process under NVT conditions (Temperature = 300 K) for 10 ps and then under NPT conditions for 100 ps using 2 fs time step, Berendsen thermostat ($\tau = 0.1$ ps) and barostat ($\tau = 2$ ps). LINCS algorithm⁵⁵ is used for bonds and the angles constriction. Further, we carry out three repeats under NPT conditions for 100 ns with Berendsen thermostat (Temperature = 300 K, $\tau = 0.1$ ps) Parrinello-Rahman barostat (Pressure = 1 bar, $\tau = 2$ ps) and using a time step of 2 fs. The integrate Newton’s equation of motion is done by using a leap-frog algorithm. A cut-off of 1.0 nm is used for both van der Waals (VDW) interaction and short-range electrostatic interaction. Particle mesh Ewald (PME)⁴³ method is employed to deal with the long-range electrostatic interactions. The configuration trajectories are output every 1 ps.

3.2 LPH for molecular aggregation and hydrogen-bonding networks

In this section, localized persistent homology is used to explore the topological fingerprint of molecular aggregation and hydrogen-bonding network at a local scale. We systematically study the osmolyte and water molecular aggregation patterns within a certain local domain, specified by a sphere with a radius from 7Å to 15 Å. The corresponding PBNs and PEs are used to quantitatively characterize the intrinsic local topology information.

Computationally, in TMAO systems, there are 63, 125, 204, 290, 400, 533, 700 and 887 TMAO molecules with 3000 water molecules from concentration 1M to 8M, respectively. In urea systems, there are 60, 120, 192, 267, 352, 450, 555 and 681 urea molecules with 3000 water molecules respectively. To analyze the topology in molecular aggregation and hydrogen-bonding networks, the TMAO and urea molecules are coarse-grained as their nitrogen and carbon atoms, respectively. The water molecules are coarse-grained as their oxygen atoms. Since the configuration data is obtained from an NPT simulation, the size of simulation box is allowed to adjust for each configuration to attain equilibrium conditions. Periodic boundary condition is used in the specification of local domains. For each simulation, we consider 101 frames (or configurations) sampled at equal intervals from the simulation trajectory. Our topological analysis is performed on these 101 frames.

3.2.1 LPH based topological features of two types of osmolytes

To facilitate an intuitive understanding of local topological information of molecular aggregation, we demonstrate the persistent barcodes calculated from TMAO and urea systems with a cutoff radius of $R_c = 9\text{\AA}$. More specifically, we consider the last configurations of the MD simulations from four different concentrations. An osmolyte molecule is randomly chosen from these last frames and its neighbouring osmolyte molecules located

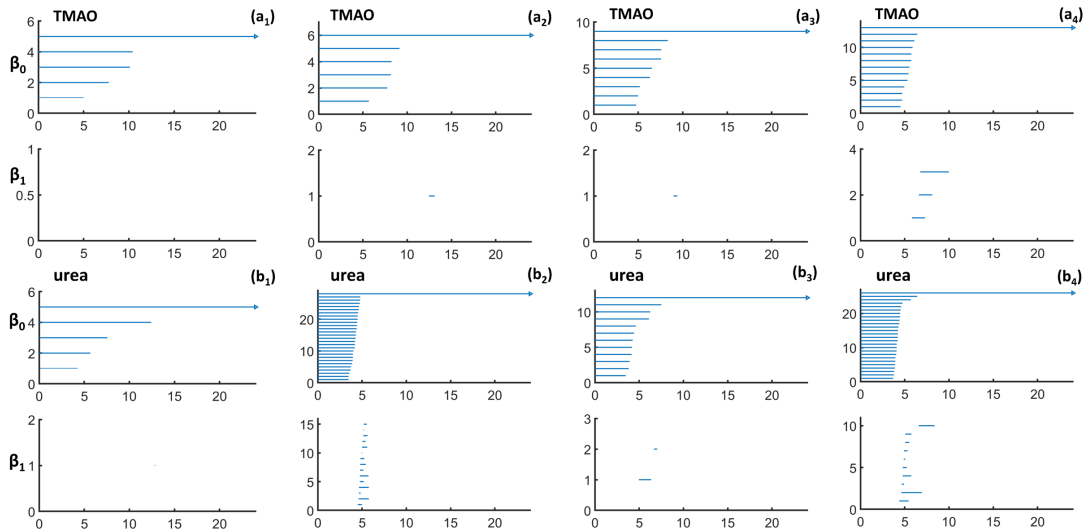


Figure 3: The local persistent barcodes for TMAO and urea aggregation. TMAO and urea molecules are coarse-grained as their nitrogen and carbon atoms. The barcodes are generated from a randomly picked molecule at the last frame of the simulation. A cutoff radius of 9\AA is used. Four different concentrations, i.e., 2M, 4M, 6M, and 8M are considered. Roughly speaking, both β_0 and β_1 bars tend to increase with the concentration.

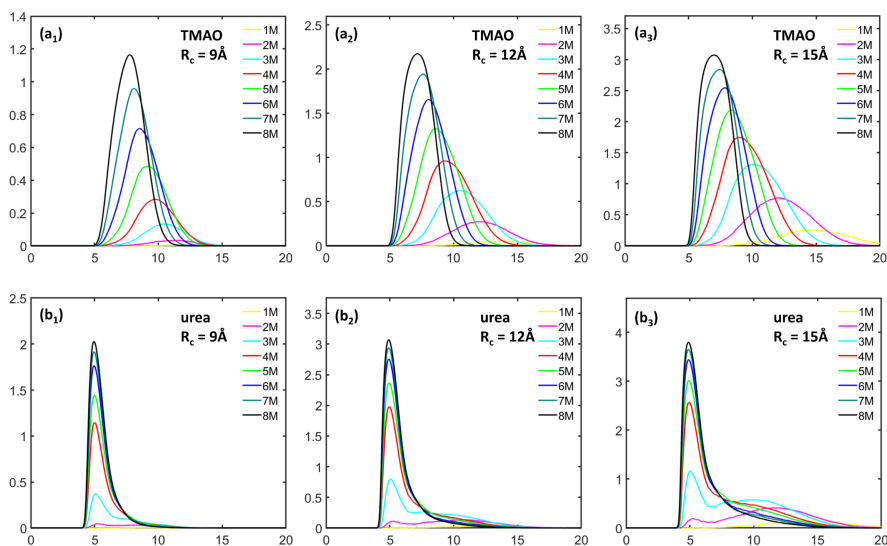


Figure 4: The comparison of average β_1 PBNs for TMAO and urea using three different cutoff radii namely, $R_c = 9\text{\AA}$, 12\AA and 15\AA respectively. The β_1 PBNs are averaged over all the frames and all molecules in each frame. It can be seen that, TMAO and urea show dramatically different local topological characteristics.

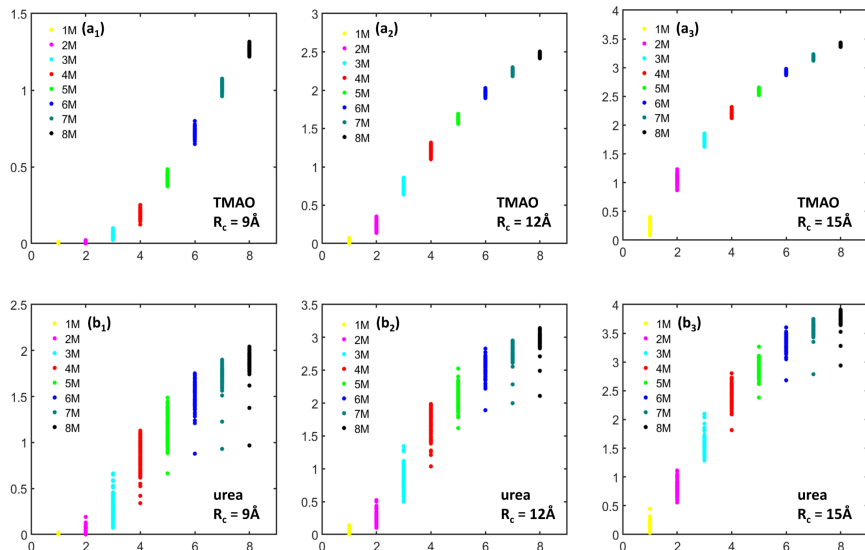


Figure 5: The comparison of average persistent entropies for TMAO and urea using three different cutoff radii, i.e., $R_c = 9\text{\AA}$, 12\AA and 15\AA . The PEs are averaged over all the molecules in each frames, thus a total 101 PEs are obtained for each simulation. It can be seen that, for a small cutoff radius of $R_c = 9\text{\AA}$, both TMAO and urea PEs at 1M are almost all zero. Further, the average PEs for both systems increase with the concentration, but their PE variances have very different properties. The TMAO PE variance decreases with concentration while urea PE variance increases.

within the cutoff radius $R_c = 9\text{\AA}$ are also selected. Persistent homology analysis is then applied on these selected molecules. The results from TMAO and urea systems are demonstrated in Figures 3. In both TMAO and urea, the total number of β_0 bars roughly increase with concentration (M), indicating the aggregation of neighboring molecules with the concentration. The β_1 bars also seem to appear more and more frequently with the increase of the concentration.

All the above results are based on a randomly picked molecule in the last frames of the simulation trajectories and can not characterize the overall behavior very well. To have a better comparison, we consider the ensemble average. More specifically, for each frame, the local persistent barcode from each molecule is calculated and then averaged. It should be noticed that we use the periodic boundary condition to include all “neighboring” molecules. This process is repeated for all 101 frames in each trajectory. We represent each persistent barcode as their PBN and PE. These PBNs are then averaged over all the frames and all the molecules in each frames to generate a single PBN for each simulation or trajectory. The PEs are averaged over all the molecules in each frame, so that a total 101 PEs are obtained from each simulation.

Figure 4 shows the β_1 PBNs obtained for the TMAO and urea system at eight different concentrations, under three different cutoff radii, i.e., $R_c = 9\text{\AA}$, 12\AA and 15\AA , respectively. As stated above, β_1 bars represent the ring, circle and loop structures in the systems. For TMAO systems, at each cutoff radius, the peak value of the local β_1 PBNs systematically increases with the concentration, indicating more and more circle structures are generated. At the same time, the position of these peak values shifts from around 13\AA to 7\AA , meaning that the size of circles systematically decreases. When we consider larger cutoff radii, similar topological patterns are observed. However, PBNs from lower concentration systems increase much faster, even though all PBNs increase with the cutoff radius. This results indicate that for lower concentration systems, there exists large-sized topological features that can not be well characterized by LPH with a small cutoff radius. For urea systems, their PBNs have a dramatically different behavior in comparison with TMAO. Roughly speaking, there are two types of peak for urea systems, especially urea systems at lower concentrations. One type of peak is located around 5\AA , and the other is around 10\AA to 12\AA . The peak at 5\AA appears even at very low concentrations and its magnitude keeps increasing with the concentration rise. The shape of this peak is much narrower than that of those of TMAO PBNs. The second type of peak can only be well observed at lower

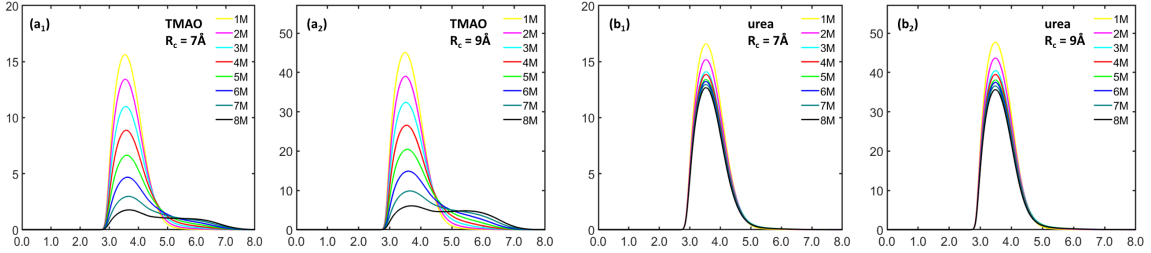


Figure 6: The comparison of average β_1 PBNs for hydrogen bonding networks from TMAO and urea using two different cutoff radii, i.e., $R_c = 7\text{\AA}$ and $R_c = 9\text{\AA}$. The coarse-grained representation of water as its oxygen atom is considered. The PBNs are averaged over all the molecules and configuration numbers. It can be seen that, TMAO and urea show very different topological characteristics.

concentrations. It has much smaller magnitude compared with that of the first type of peak.

From Figure 4, we can see that TMAO and urea demonstrate dramatically different local topological characteristics. Essentially, TMAO shows a regular local network structure. The size and total number of the circle structures from these networks consistently decrease and increase with the concentration, respectively. In contrast, urea shows a cluster-like local aggregations. Urea molecules form local clusters, whose size stays relative consistent but the total number consistently increases with concentration. Compared with our results from persistent homology analysis of the whole system,¹⁰⁵ LPH focuses more on the local topological information and systematically attenuates the influence from global topological features.

Other than PBNs, we can also calculate PEs from the LPH barcodes and use them to characterize the “topological regularity”. Figure 5 demonstrates the β_1 PEs for both TMAO and urea at eight concentrations and three cutoff radii as stated above. Note that for each simulation or trajectory, we consider 101 configurations or frames and generate 101 β_1 PEs. It can be seen that, at a small cutoff radius, the PE values from 1 M concentration system is almost all zeros, meaning that there is almost no circle structures at local scale. This is consistent with the PBN profile in Figure 4. Further, the average PE value increases systematically with the concentration for both TMAO and urea. However, the PE variance shows a very different behavior. With the concentration increase, the TMAO PE variance systematically decreases, while urea PE variance consistently increases. These results are also consistent with our findings from persistent homology analysis of the whole system.¹⁰⁵ Essentially, with the concentration increase, all osmolyte systems become topological more and more disordered. However, the variation of topological regularity for each trajectory decreases in TMAO systems but increases in urea systems.

3.2.2 LPH based topological features of hydrogen-bonding networks

In our hydrogen-bonding network analysis, we only consider the topological features for water molecules at a local scale. Similar to osmolyte systems, LPH analysis is carried out for each water molecule together with its neighbours located within a cutoff radius R_c . For each frame, we systematically go over all the 3000 water molecules and calculate 3000 local persistent barcodes. Again periodic boundary condition is considered to include all “neighboring” water molecules. The process is repeated over all the 101 frames in each trajectory. A single β_1 PBN is generated for each simulation by averaging β_1 PBNs over all the 101 frames and all the 3000 water molecules in each frame. The β_1 PEs are averaged over the 3000 water molecules in each frame, so that a total 101 β_1 PEs are obtained from each simulation. Two cutoff radii, i.e., $R_c = 7\text{\AA}$ and $R_c = 9\text{\AA}$, are considered in our LPH analysis.

Figure 6 shows the comparison of average β_1 PBNs for TMAO and urea hydrogen-bonding networks. For TMAO systems, it can be seen that their PBNs have a peak value located at around 3.5\AA . With the concentration increase, the peak value of TMAO PBNs gradually decreases. In the meantime, there is a consistent rise of the PBN values in the range from around 4.5\AA to 7.0\AA . Even though all PBNs significantly increase with the cutoff radius, the general PBN profile pattern from eight different concentrations is highly consistent. Similar to TMAO, urea PBNs also have a peak value at filtration value 3.5\AA . The peak value slightly decreases with the concentration increase. Further, the general PBN profile pattern from eight different

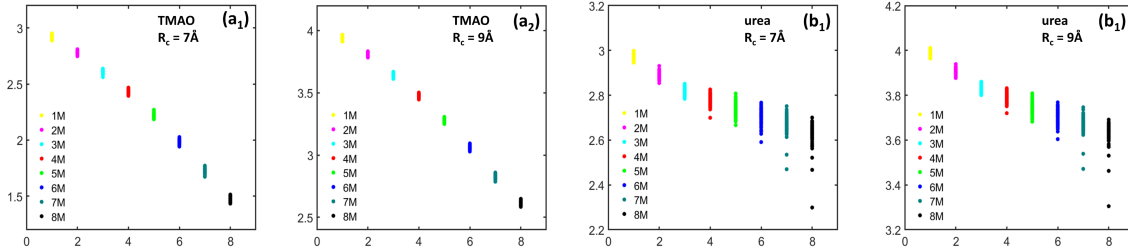


Figure 7: The comparison of average β_1 PEs for hydrogen-bonding networks from TMAO and urea systems using two different cutoff radii, i.e., $R_c = 7\text{\AA}$ and $R_c = 9\text{\AA}$. The PEs are averaged over all the water molecules in each frames, thus a total 101 PEs are obtained for each simulation. It can be seen that, the average PE decreases with the concentration for both TMAO and urea. However, the PE variance for urea systematically increases.

concentrations shares a remarkable similarity at two different local scales, even though the PBN peak values are systematically increased.

From Figure 6, we can see that TMAO and urea hydrogen-bonding networks demonstrate dramatically different local topological characteristics. For TMAO hydrogen-bonding networks, with the concentration increase, there is a systematical decrease of small-sized circle structures as well as an increase of relatively large-sized circle structures. For urea hydrogen-bonding networks, there is only a slight decrease of small-sized circle structures and no significantly increase of large-sized circle structures. More interestingly, if we compare the our LPH results with the ones from the whole hydrogen-bonding network in both ion and osmolyte systems,^{104,105} we can see that there exists a great similarity in their PBNs. Essentially, TMAO and urea hydrogen-bonding networks show two types of topological behaviors. With the concentration increase, TMAO molecules tend to destroy the local hydrogen-bonding networks, resulting a significantly increase of large circle structures. In contrast, the urea molecules have a much less impact on the hydrogen-bonding networks.

Persistent entropy from the LPH barcodes can also be used to characterize the “topological regularity” of hydrogen-bonding networks. Figure 7 demonstrates the β_1 PEs for both TMAO and urea hydrogen-bonding networks at eight concentrations and two cutoff radii. Similar to molecular aggregation analysis, for each simulation, we consider 101 configurations or frames and generate 101 β_1 PEs. It can be seen that, the average PE value for both TMAO and urea hydrogen-bonding networks decreases with the concentration increase. The same pattern is observed at two local scales. Topologically, these results indicate that both hydrogen-bonding networks become more and more regular and lattice-like with concentration increase. Note that molecular aggregation has a totally different topological behavior, their PE value systematically increases with the concentration. More interestingly, the urea PE variance is significantly larger than that of TMAO and consistently increases with the concentration. This is exactly the same as in the urea aggregation systems.

In summary, we have used LPH models to explore the osmolyte molecular aggregation and their hydrogen-bonding networks. Essentially, we separate osmolyte molecules from water molecules, and study their local topological features separately. In next section, we will focus on the interaction between osmolyte molecules and water molecules and characterize the topology of their interaction networks.

3.3 IPH based topological features for osmolyte-water interaction network

In this section, we consider both global-scale and local-scale IPHs for analyzing interactions between osmolyte molecules and water molecules. In global-scale IPH, for each osmolyte molecule, we can construct an IPH matrix from Eq.(8) with the size 3001×3001 , as there are totally 3000 water molecules. From the β_0 barcode of the IPH matrixes, a single PRDF can be calculated. And by averaging the PRDFs over all the 101 frames and all osmolyte molecules in each frame, we can obtain the average global-scale PRDF. In local-scale IPH, for each configuration or frame, an individual IPH can be constructed. Note that the size of the local-scale IPH matrix is $(N_{wtr} + N_{sml}) \times (N_{wtr} + N_{sml})$, i.e., the total number of osmolyte and water molecules in the simulation. An average local-scale PRDF (or PBN) can be evaluated by averaging their values over all the 101 frames.

Figure 8 shows the comparison of global-scale and local-scale PRDFs for both TMAO and urea systems.

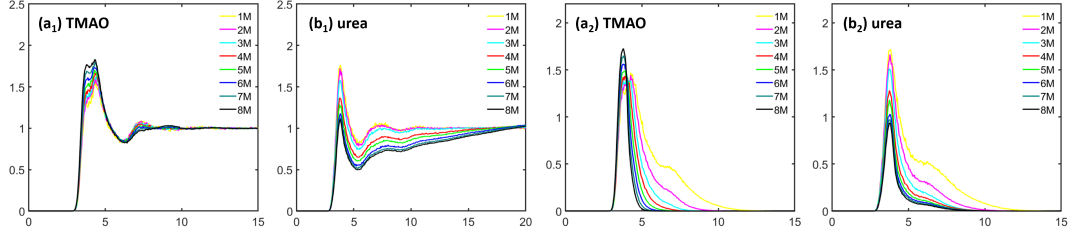


Figure 8: The comparison of global-scale and local-scale PRDFs for both TMAO and UREA. The PRDF of N-O is examined in the case of TMAO and C-O for the urea osmolyte. It can be seen that, the first peak value of the TMAO PRDFs increases with the concentration, while the first peak value of urea PRDFs decreases with the concentration.

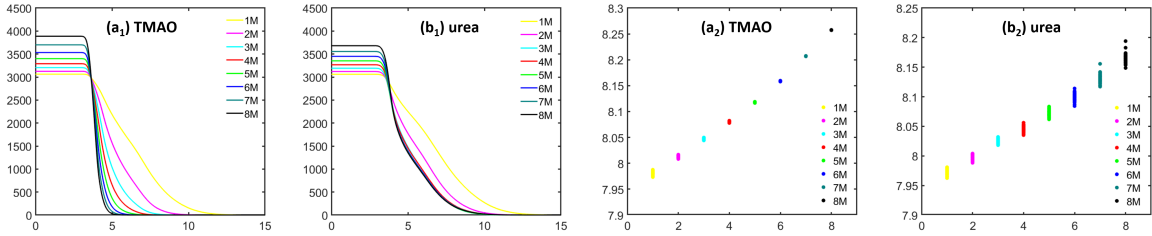


Figure 9: The comparison of average β_0 PBNs for hydrogen-bonding networks of TMAO and urea systems. The N-O pair interaction network is considered for analysis. The comparison of average β_0 PEs from the IPH analysis of TMAO and urea systems. For each configuration, a PE value can be calculated, thus a total 101 PEs are obtained for each simulation. It can be seen that, the average PE increases with the concentration for both TMAO and urea. However, the PE variance for urea systematically increases.

Both global-scale and local-scale PRDFs are normalized with the number density of the oxygen atom. The number density in global-scale is calculated by considering the number of oxygen atoms averaged over all spheres around each ion with radius r_{max} . The value of r_{max} is half the box size. In the local-scale, the number density is simply the number of oxygen atoms divided by the volume of the simulation box for a given concentration. Essentially, the global-scale PRDFs are identical to the traditional radial density functions. It can be seen that both TMAO and urea have two very obvious peaks, one located at around 4\AA and the other located at around 7\AA . However, their behaviors are dramatically different. For TMAO, the first peak value consistently increases with the concentration while the second peak value decreases with the concentration. The change of the TMAO peak values are relatively small, especially for the second peak. In contrast, both peaks of urea PRDFs vary greatly with concentration change. In local-scale IPH, PRDF values converge quickly to zero when the filtration value is larger than 12\AA , which is dramatically different from the situation in global-scale PRDFs when their values converge to 1 at large filtration value. However, the first peak of local-scale PRDFs has similar pattern as the global-scale ones. The TMAO peak value increases with concentration, while urea peak value decreases with concentration. Moreover, at the region of filtration value from 5\AA and 10\AA , which is the region for the second peak of global PRDFs, the TMAO PRDF values decrease much faster than those of urea. When the concentration is larger than 5M , nearly all TMAO PRDF values drop to zero, while urea PRDF still remain largely positive.

To have a better understanding of the local-scale PRDFs, we check the PBNs and PEs from the local-scale IPH. Figure 9 demonstrates β_0 PBNs for TMAO and urea. The β_0 PBNs are directly related to PRDFs. It can be seen that indeed the TMAO β_0 PBNs decrease much faster than those of TMAO at the filtration region from 5\AA to 10\AA , consistent with our observations in local-scale PRDFs. Further, we study the corresponding PEs. It can be seen in figure 9, that the average PE values for both local-scale IPH models increase with the concentration. More interestingly, the PE variance for TMAO IPH decreases with the concentration, while that for urea systematically increases with the concentration.

4 Conclusion

In this paper, we use the weighted persistent homology to study topological properties for osmolyte molecular aggregation and their hydrogen-bonding networks at a local scale. Two different models, i.e., localized persistent homology (LPH) and interactive persistent homology (IPH), are considered. We use persistent Betti number (PBN) and persistent entropy (PE) to quantitatively characterize the topological features from LPH and IPH. Based on persistent barcodes, we have proposed the persistent radial distribution function (PRDF). It has been found the the global-scale PRDF will reduce to traditional radial distribution function. While local-scale PRDFs can characterize the local interactions within the Voronoi cells. All these weighted persistent homology models can be used in any networks, graphs, biomolecules, etc.

Acknowledgments

This work was supported in part by Nanyang Technological University Startup Grant M4081842 and Singapore Ministry of Education Academic Research fund Tier 1 RG31/18, Tier 2 MOE2018-T2-1-033.

References

- [1] Dionysus: the persistent homology software. Software available at <http://www.mrzv.org/software/dionysus>.
- [2] M. J. Abraham, T. Murtola, R. Schulz, S. Páll, J. C. Smith, B. Hess, and E. Lindahl. GROMACS: High performance molecular simulations through multi-level parallelism from laptops to supercomputers. *SoftwareX*, 1:19–25, 2015.
- [3] M. Ahmed, B. T. Fasy, and C. Wenk. Local persistent homology based distance between maps. In *Proceedings of the 22nd ACM SIGSPATIAL International Conference on Advances in Geographic Information Systems*, pages 43–52. ACM, 2014.
- [4] I. Bakó, A. Bencsura, K. Hermansson, S. Bálint, T. Grósz, V. Chihaiia, and J. Oláh. Hydrogen bond network topology in liquid water and methanol: a graph theory approach. *Physical Chemistry Chemical Physics*, 15(36):15163–15171, 2013.
- [5] I. Bakó, T. Megyes, S. Bálint, T. Grósz, and V. Chihaiia. Water–methanol mixtures: topology of hydrogen bonded network. *Physical Chemistry Chemical Physics*, 10(32):5004–5011, 2008.
- [6] D. Bandyopadhyay, S. Mohan, S. K. Ghosh, and N. Choudhury. Molecular dynamics simulation of aqueous urea solution: is urea a structure breaker? *The Journal of Physical Chemistry B*, 118(40):11757–11768, 2014.
- [7] I. Baskakov and D. W. Bolen. Forcing thermodynamically unfolded proteins to fold. *Journal of Biological Chemistry*, 273(9):4831–4834, 1998.
- [8] I. V. Baskakov, R. Kumar, G. Srinivasan, Y. S. Ji, D. W. Bolen, and E. B. Thompson. Trimethylamine N-oxide-induced cooperative folding of an intrinsically unfolded transcription-activating fragment of human glucocorticoid receptor. *Journal of Biological Chemistry*, 274(16):10693–10696, 1999.
- [9] P. W. Bates, G. W. Wei, and Shan Zhao. Minimal molecular surfaces and their applications. *Journal of Computational Chemistry*, 29(3):380–91, 2008.
- [10] U. Bauer, M. Kerber, and J. Reininghaus. Distributed computation of persistent homology. *Proceedings of the Sixteenth Workshop on Algorithm Engineering and Experiments (ALENEX)*, 2014.
- [11] G. Bell, A. Lawson, J. Martin, J. Rudzinski, and C. Smyth. Weighted persistent homology. *arXiv preprint arXiv:1709.00097*, 2017.
- [12] P. Bendich, D. Cohen-Steiner, H. Edelsbrunner, J. Harer, and D. Morozov. Inferring local homology from sampled stratified spaces. In *Foundations of Computer Science, 2007. FOCS'07. 48th Annual IEEE Symposium on*, pages 536–546. IEEE, 2007.

- [13] P. Bendich, H. Edelsbrunner, and M. Kerber. Computing robustness and persistence for images. *IEEE Transactions on Visualization and Computer Graphics*, 16:1251–1260, 2010.
- [14] P. Bendich, E. Gasparovic, J. Harer, R. Izmailov, and L. Ness. Multi-scale local shape analysis and feature selection in machine learning applications. In *Neural Networks (IJCNN), 2015 International Joint Conference on*, pages 1–8. IEEE, 2015.
- [15] P. Bendich, B. Wang, and S. Mukherjee. Local homology transfer and stratification learning. In *Proceedings of the twenty-third annual ACM-SIAM symposium on Discrete Algorithms*, pages 1355–1370. SIAM, 2012.
- [16] H. J. C. Berendsen, D. van der Spoel, and R. van Drunen. GROMACS: a message-passing parallel molecular dynamics implementation. *Computer physics communications*, 91(1-3):43–56, 1995.
- [17] J. Binchi, E. Merelli, M. Rucco, G. Petri, and F. Vaccarino. jholes: A tool for understanding biological complex networks via clique weight rank persistent homology. *Electronic Notes in Theoretical Computer Science*, 306:5–18, 2014.
- [18] P. Bubenik. Statistical topological data analysis using persistence landscapes. *The Journal of Machine Learning Research*, 16(1):77–102, 2015.
- [19] P. Bubenik and P. T. Kim. A statistical approach to persistent homology. *Homology, Homotopy and Applications*, 19:337–362, 2007.
- [20] M. Buchet, F. Chazal, Steve Y. Oudot, and D. R. Sheehy. Efficient and robust persistent homology for measures. *Computational Geometry*, 58:70–96, 2016.
- [21] Z. X. Cang, L. Mu, and G. W. Wei. Representability of algebraic topology for biomolecules in machine learning based scoring and virtual screening. *PLoS computational biology*, 14(1):e1005929, 2018.
- [22] Z. X. Cang and G. W. Wei. Analysis and prediction of protein folding energy changes upon mutation by element specific persistent homology. *Bioinformatics*, 33(22):3549–3557, 2017.
- [23] Z. X. Cang and G. W. Wei. Integration of element specific persistent homology and machine learning for protein-ligand binding affinity prediction. *International journal for numerical methods in biomedical engineering*, page 10.1002/cnm.2914, 2017.
- [24] Z. X. Cang and G. W. Wei. TopologyNet: Topology based deep convolutional and multi-task neural networks for biomolecular property predictions. *PLOS Computational Biology*, 13(7):e1005690, 2017.
- [25] G. Carlsson. Topology and data. *Am. Math. Soc*, 46(2):255–308, 2009.
- [26] G. Carlsson, T. Ishkhanov, V. Silva, and A. Zomorodian. On the local behavior of spaces of natural images. *International Journal of Computer Vision*, 76(1):1–12, 2008.
- [27] G. Carlsson, A. Zomorodian, A. Collins, and L. J. Guibas. Persistence barcodes for shapes. *International Journal of Shape Modeling*, 11(2):149–187, 2005.
- [28] F. Cazals, F. Proust, R. P. Bahadur, and J. Janin. Revisiting the voronoi description of protein–protein interfaces. *Protein Science*, 15(9):2082–2092, 2006.
- [29] T. V. Chalikian and K. J. Breslauer. Thermodynamic analysis of biomolecules: a volumetric approach. *Current opinion in structural biology*, 8(5):657–664, 1998.
- [30] D. Chandler. *Introduction to Modern Statistical Mechanics*. Oxford University Press, 1987.
- [31] H. Chintakunta, T. Gentimis, R. Gonzalez-Diaz, M. J. Jimenez, and H. Krim. An entropy-based persistence barcode. *Pattern Recognition*, 48(2):391–401, 2015.

- [32] J. Choi and M. Cho. Ion aggregation in high salt solutions. II. spectral graph analysis of water hydrogen-bonding network and ion aggregate structures. *The Journal of chemical physics*, 141(15):154502, 2014.
- [33] J. Choi and M. Cho. Ion aggregation in high salt solutions. IV. graph-theoretical analyses of ion aggregate structure and water hydrogen bonding network. *The Journal of chemical physics*, 143(10):104110, 2015.
- [34] J. Choi and M. Cho. Ion aggregation in high salt solutions. VI. spectral graph analysis of chaotropic ion aggregates. *The Journal of chemical physics*, 145(17):174501, 2016.
- [35] J. H. Choi, H. Lee, H. R. Choi, and M. Cho. Graph theory and ion and molecular aggregation in aqueous solutions. *Annual review of physical chemistry*, 69:125–149, 2018.
- [36] J. A. B. da Silva, F. G. B. Moreira, V. M. L. dos Santos, and R. L. Longo. On the hydrogen bond networks in the water–methanol mixtures: topology, percolation and small-world. *Physical Chemistry Chemical Physics*, 13(14):6452–6461, 2011.
- [37] R. J. M. Dawson. Homology of weighted simplicial complexes. *Cahiers de Topologie et Géométrie Différentielle Catégoriques*, 31(3):229–243, 1990.
- [38] B. Di Fabio and C. Landi. A Mayer-Vietoris formula for persistent homology with an application to shape recognition in the presence of occlusions. *Foundations of Computational Mathematics*, 11:499–527, 2011.
- [39] V. M. L. dos Santos, F. G. B. Moreira, and R. L. Longo. Topology of the hydrogen bond networks in liquid water at room and supercritical conditions: a small-world structure. *Chemical physics letters*, 390(1):157–161, 2004.
- [40] H. Edelsbrunner. *Weighted alpha shapes*, volume 92. University of Illinois at Urbana-Champaign, Department of Computer Science, 1992.
- [41] H. Edelsbrunner and P. Koehl. The geometry of biomolecular solvation. *Combinatorial and computational geometry*, 52:243–275, 2005.
- [42] H. Edelsbrunner, D. Letscher, and A. Zomorodian. Topological persistence and simplification. *Discrete Comput. Geom.*, 28:511–533, 2002.
- [43] U. Essmann, L. Perera, M. L. Berkowitz, T. Darden, H. Lee, and L. G. Pedersen. A smooth particle mesh Ewald method. *The Journal of chemical physics*, 103(19):8577–8593, 1995.
- [44] B. T. Fasy, J. Kim, F. Lecci, and C. Maria. Introduction to the r package tda. *arXiv preprint arXiv:1411.1830*, 2014.
- [45] B. T. Fasy and B. Wang. Exploring persistent local homology in topological data analysis. In *Acoustics, Speech and Signal Processing (ICASSP), 2016 IEEE International Conference on*, pages 6430–6434. IEEE, 2016.
- [46] X. Feng, K. L. Xia, Y. Y. Tong, and G. W. Wei. Multiscale geometric modeling of macromolecules II: lagrangian representation. *Journal of Computational Chemistry*, 34:2100–2120, 2013.
- [47] P. Frosini and C. Landi. Persistent Betti numbers for a noise tolerant shape-based approach to image retrieval. *Pattern Recognition Letters*, 34(8):863–872, 2013.
- [48] M. Gameiro, Y. Hiraoka, S. Izumi, M. Kramar, K. Mischaikow, and V. Nanda. Topological measurement of protein compressibility via persistence diagrams. *preprint*, 2013.
- [49] P. Ganguly, P. Boserman, N. F. van der Vegt, and J. E. Shea. Trimethylamine N-oxide counteracts urea denaturation by inhibiting protein–urea preferential interaction. *Journal of the American Chemical Society*, 140(1):483–492, 2017.

- [50] P. Ganguly, T. Hajari, J. E. Shea, and N. F. A. van der Vegt. Mutual exclusion of urea and trimethylamine N-oxide from amino acids in mixed solvent environment. *The journal of physical chemistry letters*, 6(4):581–585, 2015.
- [51] P. Ganguly, N. F. van der Vegt, and J. E. Shea. Hydrophobic association in mixed urea–TMAO solutions. *The journal of physical chemistry letters*, 7(15):3052–3059, 2016.
- [52] R. Ghrist. Barcodes: the persistent topology of data. *Bulletin of the American Mathematical Society*, 45(1):61–75, 2008.
- [53] C. Giusti, R. Ghrist, and D. S. Bassett. Twos company, three (or more) is a simplex. *Journal of computational neuroscience*, 41(1):1–14, 2016.
- [54] L. Guibas, D. Morozov, and Q. Mérigot. Witnessed k-distance. *Discrete & Computational Geometry*, 49(1):22–45, 2013.
- [55] B. Hess, H. Bekker, H. J. C. Berendsen, and J. G. E. M. Fraaije. Lincs: a linear constraint solver for molecular simulations. *Journal of computational chemistry*, 18(12):1463–1472, 1997.
- [56] Y. Hiraoka, T. Nakamura, A. Hirata, E. G. Escobar, K. Matsue, and Y. Nishiura. Hierarchical structures of amorphous solids characterized by persistent homology. *Proceedings of the National Academy of Sciences*, 113(26):7035–7040, 2016.
- [57] D. Horak, S. Maletic, and M. Rajkovic. Persistent homology of complex networks. *Journal of Statistical Mechanics: Theory and Experiment*, 2009(03):P03034, 2009.
- [58] H. W. Horn, W. C. Swope, J. W. Pitera, J. D. Madura, T. J. Dick, G. L. Hura, and T. Head-Gordon. Development of an improved four-site water model for biomolecular simulations: TIP4P-Ew. *The Journal of chemical physics*, 120(20):9665–9678, 2004.
- [59] J. Hunger, N. Ottosson, K. Mazur, M. Bonn, and H. J. Bakker. Water-mediated interactions between trimethylamine-N-oxide and urea. *Physical Chemistry Chemical Physics*, 17(1):298–306, 2015.
- [60] A. Idrissi, M. Gerard, P. Damay, M. Kiselev, Y. Puhovsky, E. Cinar, P. Lagant, and G. Vergoten. The effect of urea on the structure of water: A molecular dynamics simulation. *The Journal of Physical Chemistry B*, 114(13):4731–4738, 2010.
- [61] P. M. Kasson, A. Zomorodian, S. Park, N. Singhal, L. J. Guibas, and V. S. Pande. Persistent voids a new structural metric for membrane fusion. *Bioinformatics*, 23:1753–1759, 2007.
- [62] K. M. Kast, J. Brickmann, S. M. Kast, and R. S. Berry. Binary phases of aliphatic n-oxides and water: Force field development and molecular dynamics simulation. *The Journal of Physical Chemistry A*, 107(27):5342–5351, 2003.
- [63] H Lee, H. Kang, M. K. Chung, B. Kim, and D. S. Lee. Persistent brain network homology from the perspective of dendrogram. *Medical Imaging, IEEE Transactions on*, 31(12):2267–2277, Dec 2012.
- [64] Y. T. Liao, A. C. Manson, M. R. DeLyser, W. G. Noid, and P. S. Cremer. Trimethylamine N-oxide stabilizes proteins via a distinct mechanism compared with betaine and glycine. *Proceedings of the National Academy of Sciences*, 114(10):2479–2484, 2017.
- [65] X. Liu, Z. Xie, and D. Y. Yi. A fast algorithm for constructing topological structure in large data. *Homology, Homotopy and Applications*, 14:221–238, 2012.
- [66] C. Maria. Filtered complexes. In *GUDHI User and Reference Manual*. GUDHI Editorial Board, 2015.
- [67] F. Meersman, D. Bowron, A. K. Soper, and M. H. J. Koch. An X-ray and neutron scattering study of the equilibrium between trimethylamine N-oxide and urea in aqueous solution. *Physical Chemistry Chemical Physics*, 13(30):13765–13771, 2011.

- [68] Z. Y. Meng, D. V. Anand, Y. P. Lu, J. Wu, and K. L. Xia. Weighted persistent homology for biomolecular data analysis. *arXiv preprint arXiv:1903.02890*, 2019.
- [69] E. Merelli, M. Rucco, P. Sloot, and L. Tesei. Topological characterization of complex systems: Using persistent entropy. *Entropy*, 17(10):6872–6892, 2015.
- [70] K. Mischaikow, M. Mrozek, J. Reiss, and A. Szymczak. Construction of symbolic dynamics from experimental time series. *Physical Review Letters*, 82:1144–1147, 1999.
- [71] K. Mischaikow and V. Nanda. Morse theory for filtrations and efficient computation of persistent homology. *Discrete and Computational Geometry*, 50(2):330–353, 2013.
- [72] J. R. Munkres. *Elements of algebraic topology*. CRC Press, 2018.
- [73] Vidit Nanda. Perseus: the persistent homology software. Software available at <http://www.sas.upenn.edu/~vnanda/perseus>.
- [74] D. D. Nguyen, Z. X. Cang, K. D. Wu, M. L. Wang, Y. Cao, and G. Wei. Mathematical deep learning for pose and binding affinity prediction and ranking in D3R Grand Challenges. *Journal of computer-aided molecular design*, 33(1):71–82, 2019.
- [75] D. D. Nguyen, T. Xiao, M. L. Wang, and G. W. Wei. Rigidity strengthening: A mechanism for protein–ligand binding. *Journal of chemical information and modeling*, 57(7):1715–1721, 2017.
- [76] P. Niyogi, S. Smale, and S. Weinberger. A topological view of unsupervised learning from noisy data. *SIAM Journal on Computing*, 40:646–663, 2011.
- [77] A. Oleinikova, N. Smolin, I. Brovchenko, A. Geiger, and Roland Winter. Formation of spanning water networks on protein surfaces via 2D percolation transition. *The journal of physical chemistry B*, 109(5):1988–1998, 2005.
- [78] D. Pachauri, C. Hinrichs, M.K. Chung, S.C. Johnson, and V. Singh. Topology-based kernels with application to inference problems in alzheimer’s disease. *Medical Imaging, IEEE Transactions on*, 30(10):1760–1770, Oct 2011.
- [79] A. Panuszko, P. Bruzdziak, J. Zielkiewicz, D. Wyrzykowski, and J. Stangret. Effects of urea and trimethylamine-N-oxide on the properties of water and the secondary structure of hen egg white lysozyme. *The Journal of Physical Chemistry B*, 113(44):14797–14809, 2009.
- [80] S. Paul and G. N. Patey. Structure and interaction in aqueous urea-trimethylamine-N-oxide solutions. *Journal of the American Chemical Society*, 129(14):4476–4482, 2007.
- [81] D. A. Pearlman, D. A. Case, J. W. Caldwell, W. S. Ross, T. E. Cheatham III, S. DeBolt, D. Ferguson, G. Seibel, and P. Kollman. AMBER, a package of computer programs for applying molecular mechanics, normal mode analysis, molecular dynamics and free energy calculations to simulate the structural and energetic properties of molecules. *Computer Physics Communications*, 91(1-3):1–41, 1995.
- [82] M. Petřek, P. Košinová, J. Koča, and M. Otyepka. MOLE: a voronoi diagram-based explorer of molecular channels, pores, and tunnels. *Structure*, 15(11):1357–1363, 2007.
- [83] G. Petri, M. Scolamiero, I. Donato, and F. Vaccarino. Topological strata of weighted complex networks. *PloS one*, 8(6):e66506, 2013.
- [84] C. S. Pun, K. L. Xia, and S. X. Lee. Persistent-homology-based machine learning and its applications—a survey. *arXiv preprint arXiv:1811.00252*, 2018.
- [85] T. P. Radhakrishnan and W. C. Herndon. Graph theoretical analysis of water clusters. *The Journal of Physical Chemistry*, 95(26):10609–10617, 1991.

- [86] S. Q. Ren, C. Y. Wu, and J. Wu. Weighted persistent homology. *Rocky Mountain Journal of Mathematics*, 48(8):2661–2687, 2018.
- [87] Y. L. A. Rezus and H. J. Bakker. Effect of urea on the structural dynamics of water. *Proceedings of the National Academy of Sciences*, 103(49):18417–18420, 2006.
- [88] B. Rieck, H. Mara, and H. Leitte. Multivariate data analysis using persistence-based filtering and topological signatures. *IEEE Transactions on Visualization and Computer Graphics*, 18:2382–2391, 2012.
- [89] J. Rosgen and R. Jackson-Atogi. Volume exclusion and H-bonding dominate the thermodynamics and solvation of trimethylamine-N-oxide in aqueous urea. *Journal of the American Chemical Society*, 134(7):3590–3597, 2012.
- [90] P. J. Rossky. Protein denaturation by urea: slash and bond. *Proceedings of the National Academy of Sciences*, 105(44):16825–16826, 2008.
- [91] M. Rucco, F. Castiglione, E. Merelli, and M. Pettini. Characterisation of the idiotypic immune network through persistent entropy. In *Proceedings of ECCS 2014*, pages 117–128. Springer, 2016.
- [92] M. Saadatfar, H. Takeuchi, V. Robins, N. Francois, and Y. Hiraoka. Pore configuration landscape of granular crystallization. *Nature communications*, 8:15082, 2017.
- [93] C. J. Sahle, M. A. Schroer, I. Juurinen, and J. Niskanen. Influence of TMAO and urea on the structure of water studied by inelastic X-ray scattering. *Physical Chemistry Chemical Physics*, 18(24):16518–16526, 2016.
- [94] V. D. Silva and R. Ghrist. Blind swarms for coverage in 2-d. In *In Proceedings of Robotics: Science and Systems*, page 01, 2005.
- [95] G. Singh, F. Memoli, T. Ishkhanov, G. Sapiro, G. Carlsson, and D. L. Ringach. Topological analysis of population activity in visual cortex. *Journal of Vision*, 8(8), 2008.
- [96] N. Smolin, V. P. Voloshin, A. V. Anikeenko, A. Geiger, R. Winter, and N. N. Medvedev. TMAO and urea in the hydration shell of the protein snase. *Physical Chemistry Chemical Physics*, 19(9):6345–6357, 2017.
- [97] Andrew Tausz, Mikael Vejdemo-Johansson, and Henry Adams. Javaplex: A research software package for persistent (co)homology. Software available at <http://code.google.com/p/javaplex>, 2011.
- [98] H. C. Tseng and D. J. Graves. Natural methylamine osmolytes, trimethylamine N-oxide and betaine, increase tau-induced polymerization of microtubules. *Biochemical and biophysical research communications*, 250(3):726–730, 1998.
- [99] V. N. Uversky, J. Li, and A. L. Fink. Trimethylamine-N-oxide-induced folding of α -synuclein. *FEBS letters*, 509(1):31–35, 2001.
- [100] B. Wang, B. Summa, V. Pascucci, and M. Vejdemo-Johansson. Branching and circular features in high dimensional data. *IEEE Transactions on Visualization and Computer Graphics*, 17:1902–1911, 2011.
- [101] B. Wang and G. W. Wei. Object-oriented persistent homology. *Journal of Computational Physics*, 305:276–299, 2016.
- [102] Chengyuan Wu, Shiquan Ren, Jie Wu, and Kelin Xia. Weighted (co) homology and weighted laplacian. *arXiv preprint arXiv:1804.06990*, 2018.
- [103] K. D. Wu and G. W. Wei. Quantitative toxicity prediction using topology based multi-task deep neural networks. *Journal of chemical information and modeling*, page 10.1021/acs.jcim.7b00558, 2018.

- [104] K. L. Xia. Persistent homology analysis of ion aggregations and hydrogen-bonding networks. *Physical Chemistry Chemical Physics*, 20(19):13448–13460, 2018.
- [105] K. L. Xia, D. V. Anand, S. Saxena, and Y. G. Mu. Persistent homology analysis of osmolyte molecular aggregation and their hydrogen-bonding networks. *arXiv preprint [arXiv:1905.11800](https://arxiv.org/abs/1905.11800)*, 2019.
- [106] K. L. Xia, X. Feng, Y. Y. Tong, and G. W. Wei. Multiscale geometric modeling of macromolecules i: Cartesian representation. *Journal of Computational Physics*, 275:912–936, 2014.
- [107] K. L. Xia, X. Feng, Y. Y. Tong, and G. W. Wei. Persistent homology for the quantitative prediction of fullerene stability. *Journal of Computational Chemistry*, 36:408–422, 2015.
- [108] K. L. Xia, Z. M. Li, and L. Mu. Multiscale persistent functions for biomolecular structure characterization. *Bulletin of mathematical biology*, 80(1):1–31, 2018.
- [109] K. L. Xia and G. W. Wei. Persistent homology analysis of protein structure, flexibility and folding. *International Journal for Numerical Methods in Biomedical Engineering*, 30:814–844, 2014.
- [110] K. L. Xia and G. W. Wei. Persistent homology analysis of protein structure, flexibility, and folding. *International journal for numerical methods in biomedical engineering*, 30(8):814–844, 2014.
- [111] K. L. Xia and G. W. Wei. Multidimensional persistence in biomolecular data. *Journal Computational Chemistry*, 36:1502–1520, 2015.
- [112] K. L. Xia and G. W. Wei. Persistent topology for cryo-EM data analysis. *International Journal for Numerical Methods in Biomedical Engineering*, 31:e02719, 2015.
- [113] K. L. Xia, Z. X. Zhao, and G. W. Wei. Multiresolution persistent homology for excessively large biomolecular datasets. *The Journal of chemical physics*, 143(13):10B603_1, 2015.
- [114] W. J. Xie, S. Cha, T. Ohto, W. Mizukami, Y. Mao, M. Wagner, M. Bonn, J. Hunger, and Y. Nagata. Large hydrogen-bond mismatch between TMAO and urea promotes their hydrophobic association. *Chem*, 4(11):2615–2627, 2018.
- [115] Y. Yao, J. Sun, X. H. Huang, G. R. Bowman, G. Singh, M. Lesnick, L. J. Guibas, V. S. Pande, and G. Carlsson. Topological methods for exploring low-density states in biomolecular folding pathways. *The Journal of Chemical Physics*, 130:144115, 2009.
- [116] S. G. Zetterholm, G. A. Verville, L. Boutwell, C. Boland, J. C. Prather, J. Bethea, J. Cauley, K. E. Warren, S. A. Smith, D. H. Magers, et al. Noncovalent interactions between Trimethylamine N-Oxide (TMAO), urea, and water. *The Journal of Physical Chemistry B*, 122(38):8805–8811, 2018.
- [117] A. Zomorodian and G. Carlsson. Computing persistent homology. *Discrete Comput. Geom.*, 33:249–274, 2005.